Dynamic light scattering at a growing crystal interface: Ice-water system

J. P. Vesenka and Y. Yeh
Department of Applied Science, University of California, Davis, California 95616
(Received 28 January 1988; revised manuscript received 4 May 1988)

We have examined quasielastic light scattering off the crystal-melt interface of growing ice crystals using photon correlation spectroscopy. The intensity autocorrelation spectra exhibit two exponential decay rates with vastly different time constants. The fast decay is found only during growth and is similar to that observed by Bilgram and his co-workers. We have found several new features associated with the slow-decay component: (1) nonzero intercept of the decay constant Γ versus the square of the scattering vector q^2 during growth; (2) a liftoff layer that depends on the type of gaseous impurity; and (3) a direct relationship between the effective hydrodynamic radius of the slow component and the degree of its size polydispersity. These provide new evidence to support Cummins's hypothesis that this component of the spectrum is caused by the segregation and precipitation of tiny gas bubbles at the crystal's surface.

I. INTRODUCTION

The dynamics of crystal growth from the melt is an important, but poorly understood, process. Recently light scattering techniques, including photon correlation spectroscopy, have been used to examine this problem. Using laser light, Bilgram, Güttinger, and Känzig[1] were the first to observe anomalous Rayleigh scattering off the surface of growing ice crystals in 1978. They reported that quasielastically scattered light from the surface of pure ice crystals growing into its melt exhibited correlated intensity fluctuations characteristic of relaxational scattering. That is, the intensity autocorrelation function, $C^{(2)}(\tau)$, exponentially decreased in time τ with decay constant, or linewidth Γ,

$$C^{(2)}(\tau)=\langle I(t)I(t+\tau)\rangle = A+Be^{-2\Gamma\tau}, \quad (1)$$

where A and B are constants. The intensity of this quasielastically scattered light is much greater than that from either the bulk melt or the single crystal, and Γ was found to be proportional to the scattering vector squared q^2. Here $q=(4\pi n/\lambda)\sin(\theta/2)$, where n is the index of refraction of water, λ is the wavelength of incident light in vacuum, and θ is the scattering angle. This linear behavior in Γ versus q^2 is typical of diffusive scattering mechanisms with the slope being the z-averaged diffusion coefficient D.[2] The linewidths found by Bilgram, Güttinger, and Känzig were independent of the growth rate and temperature gradient employed in their experiments. Rayleigh scattered light has since been observed in other crystals (cyclohexanol, salol, byphenyl, and naphthalene).[3–8]

Our recent experimental observations suggest that light scattering during the growth of ice crystals may be a result of two different phenomena. The linewidths observed by Bilgram's group are at least ten times larger than those of Brown *et al.*[9] who looked at scattering from a different crystal axis (**a** axis). Our present experiments have been performed with crystals grown in the same direction as Bilgram's (**c** axis) and show evidence of two different types of relaxational scattering, that is, both fast and slow transients. The fast transient may be uniquely associated with growth parallel to the **c** axis of ice. The slower relaxational scattering is not unique to crystal growth and is similar to scattering that has been observed in a variety of crystal systems besides ice. Cummins has suggested this slow transient is caused by the random motion of gas-impurity microbubbles that are confined to the surface of a growing crystal.[3]

Cummins's microbubble hypothesis has practical consequences in the study of crystal growth processes. The precipitation and incorporation of gaseous impurities at the surface of a growing crystal affects the crystal's optical and mechanical properties. Assuming the scattering is caused by a dilute system of microbubbles undergoing Brownian motion on the crystal surface, we can determine the average hydrodynamic radius from the Stokes-Einstein relationship: $r_h=kT/6\pi\eta D$, where k is Boltzmann's constant, T the absolute temperature, and η the viscosity of water.[2] Since our autocorrelation spectra do not perfectly fit to a single exponential decay, the quadratic coefficient of the cumulant analysis records the deviation about the average linewidth

$$\mu_2=\int G(\Gamma)(\Gamma-\langle\Gamma\rangle)^2 d\Gamma, \quad (2)$$

where $G(\Gamma)$ is the normalized distribution of decay rates and $\langle\Gamma\rangle$ is the average linewidth. Again, using the microbubble picture as our model, the second cumulant is a measure of the distribution of bubble sizes on the surface, also called the polydispersity. We provide new evidence supporting the suggestion that the source of the slow scattering process is the result of residual gaseous impurities trapped on the solid-liquid interface during crystal growth.

II. EXPERIMENTAL

The crystal purification procedure, apparatus, and spectroscopic technique have been described by Brown *et al.*[9] The sample cells were redesigned (Pyrex tubes

12.7 cm long by 1.0 cm inner diameter) to accept snug-fit cylindrical crystal seeds. The earlier paraffin wrapper used to cap the cells was replaced by stainless-steel lids with ethylene propylene *O* rings. These new seals have the advantage of being airtight, improving our ability to control the atomsphere in which the crystals are exposed. Preparation of ice crystals with the c axis oriented parallel to the growth direction is similar to Güttinger, Bilgram, and Känzig[10] with the following modification: Our cold room is the freezer compartment of a refrigerator ($63\times26\times45\text{cm}^3$) where a small lathe is accessible through gloves mounted on a Plexiglass-windowed cold shield.

The most significant change in this purification procedure was the control of gaseous contamination in our ice crystals. This was performed after each zone refinement was carried out by decanting sample impurities in a helium-filled work box. This sealed Plexiglass box ($76\times30\times33$ cm^3) was designed to maintain a positive pressure of slightly soluble inert gas inside. The work was kept dust free by locating it inside our laminar flow bench where the air is filtered to 0.3 μm. The samples were accessed through the portable glove-mounted unit mentioned above.

Before the helium-filled work box was employed our autocorrelation spectra revealed only the slow scattering component. Subsequently large linewidths ($\langle\Gamma\rangle\approx1000$ s^{-1}) were recorded from growing crystals, but only after the samples were prepared under the above strictly controlled atmospheric conditions. This appears to be the weaker scattering of the fast component originally found by Bilgram and co-workers. The fact that the slow component disappears when gaseous impurities are excluded using these rigorous measures suggest to us that the slow relaxational scattering is gaseous in origin.

Because we suspected that the source of the slow-decay spectra was from tiny gas bubbles we subjected our samples to the extreme condition of bubble saturation. Our experimental apparatus was altered to allow the insertion of high purity (99.999%) helium or argon gas through a 0.22-μm filter and a hypodermic needle in the melt. The inert gas was bubbled for an hour to ensure saturation in the water (at 0°C and 1 atm for He: 0.94 cm^3/100 cm^3 water, for Ar: 5.6 cm^3/100 cm^3).[11] Gas that was not dissolved into the water was effective in purging the outer chamber of the growth apparatus of ambient atmospheric gases. The bubbling process stirred the liquid and melted the crystal considerably below its static equilibrium position. After gas injection of the melt was completed, the inert gas was routed into the outer chamber to avoid back filling with laboratory air. We relocated the level of the crystal-melt interface to the center of the temperature gradient. This procedure prevented rapid crystal growth from occurring as the crystal returned to its equilibrium position. Measurements were taken after an hour of either static or steady-state growth conditions.

Rapid autocorrelation measurements taken from the crystal surface were facilitated by improved scattering collection optics and remote control of the mechanically driven beam steering apparatus. The last step before conducting an experiment involved checking for bright, forward scattering from particulate impurities with a laser beam. An experiment was started only in the absence of impurity scattering. Although our crystals would satisfy this criterion, scatterers frequently appeared in the melts. Originally we had a single linear temperature gradient along the length of a cell which separated the crystal into a solid portion in the bottom half and its melt above it. We were concerned about possible contamination of the melt from impurities that had been lodged on the top of the crystal during the final zone refinement pass. Addition of a second cooling block directly above the heater made it possible to keep the top of the crystal frozen, emulating a true zone-melt setup. Consequently, any impurities introduced during the last decanting of the melt remained frozen into the outer region of the crystal. This apparatus was successful in maintaining an "intermediate melt zone" free of surface contaminants.

III. RESULTS

A. Spectral components

We have separated two different decay constants in our autocorrelation spectra. The scattered light is collected normal to the incident laser beam, approximately in the plane of the growing crystal. The fast-decay component had an average linewidth $\langle\Gamma\rangle\approx1000$ s^{-1} and was observed only during crystal growth. Prior to control of the ambient atmosphere to which the samples were exposed, only the slow component was observed. This component had a decay constant that varied between 1 to 100 s^{-1}. Slow relaxational spectra were recorded both during steady-state growth and melting, in static equilibrium *before* crystal growth was initiated, and in samples with the melt zone in the center of the crystal. The slow component was characterized by the following observations.

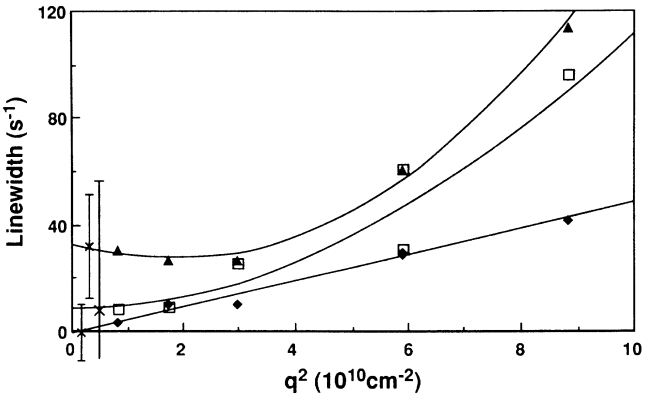

FIG. 1. Angular dependence of the linewidth during various static or nonequilibrium steady-state conditions (♦, before growth was initiated; ▲, during crystal growth; □, after growth was arrested; × are the extrapolated intercepts). The error bars associated with these intercepts (offset from zero for clarity) represent a statistical confidence limit of 95%. Each data point is arrived at by cumulants analysis of the autocorrelation spectra, truncated at the quadratic term. Both the linear coefficient (linewidth) and the scattering vector squared have a 1% systematic error.

B. Nonlinearity of Γ versus q^2

Within experimental error, the linewidths in most of the crystal systems examined by light scattering have been found to be proportional to the scattering vector squared.[1,3–9] Under static pre- or post-growth conditions, linear plots of our Γ versus q^2 data extrapolated to zero scattering angle reveal a negative intercept (Fig. 1; ♦, □). This is result is consistent with a highly polydisperse scattering medium when fitted to a single averaged decay constant. However, during steady-state growth (Fig. 1; ▲) there is some indication that the dependence on q is not strictly quadratic. Extrapolation of this data to $\mathbf{q}=\mathbf{0}$ yielded a positive y intercept during growth, suggesting an effective nonzero decay constant, $\Gamma_{q=0}$. These intercepts were more pronounced for large average bubble radius (in Fig. 1, $r_h \approx 2$ μm). The error bars represent statistical confidence limits (95% level) for the extrapolated values.

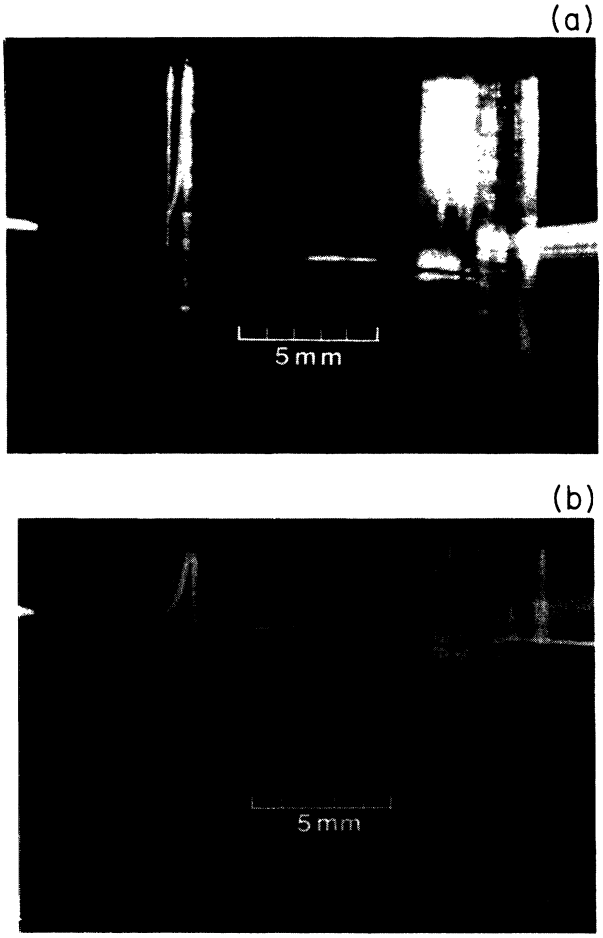

FIG. 2. (a) A crystal at the bottom of the picture is growing into its melt on top (magnification $\approx \times 4$). The crystal surface is the faintly visible concave-down structure appearing horizontally across the center of the photo. The bright white spot in the middle is the 488-nm-wavelength laser beam scattered off the microbubbles in the center of our cell. The straight line entering from the left and reflecting off the surface to the right is the beam as it undergoes Raman scattering from the clear water. (b) Photo of the same cell as in (a) taken 3 min after the ice surface was raised into above-freezing conditions. A liftoff layer of microbubbles appears as the crystal substrate melts underneath a continuous layer of scatterers. A 1-mm gap between the liftoff layer and the surface of the crystal can be seen. There are no scatterers on the surface of the receding crystal; the scattered light observed from the crystal surface represents specular reflection of scattering from the liftoff layer. The temperature gradient is about 10° C/cm.

C. Liftoff layer

McDonaugh (unpublished data, 1985) initially observed that after a layer of scatterers had developed on the crystal surface, a "liftoff layer" would appear above the melting crystal substrate. We have made similar observations in the unadulterated water samples [Figs. 2(a) and 2(b)]. The persistence time of the liftoff layer was approximately 10 min, and it had a thickness up to 0.2 mm [Fig. 2(b)]. A similar phenomenon has been reported for the cyclohexanol system.[7] If the "scattering layer" appeared continuous to the eye, then we observed that the crystal surface would melt back virtually free of any quasielastic scattering. In contrast, when scattering was localized in "islands," the melting crystal surface continued to exhibit dynamic scattering. Quite different results were obtained in the gas injected samples, in which those injected with helium, but not argon, exhibited a liftoff layer.

D. Hydrodynamic radius and polydispersity

We have found a direct correlation between the normalized polydispersity, defined by $P=\mu_2/\langle\Gamma\rangle^2$, and the average effective hydrodynamic radius r_h. This relationship was less conspicuous in the unadulerated samples in which the concentration of scatterers was relatively low. However, this correction was easily observed in the gas-injected samples where bubbles were super-abundant (Fig. 3). This effect is highly dependent on the location of

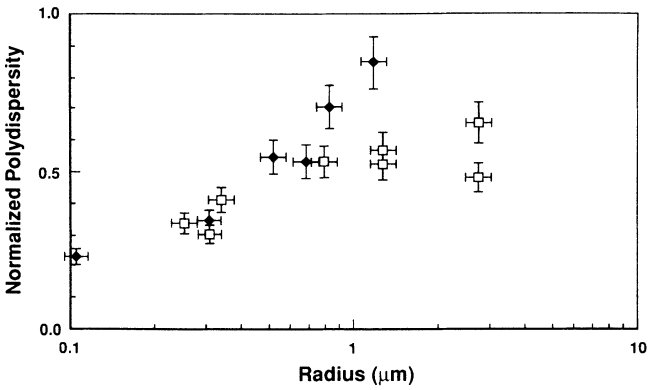

FIG. 3. In samples injected with either argon (□) or helium (♦) gas, a range of normalized polydispersity was found at different locations of the growing surface. The polydispersity continues to increase with increasing average hydrodynamic radius in helium injected samples but levels off for argon injected samples.

scattering on the crystal surface since a wide range of P and r_h values may be found by probing different sections of the surface at any time. Measurements taken from different locations on the same crystal surface showed the radii varied by a factor of approximately 100 and the normalized polydispersity differed by up to 100% of the average radii. These radii were comparable to those obtained from the unadulterated samples. Note that the data for argon reaches a plateau where the polydispersity no longer increases with average bubble size while the data for helium does not level off.

IV. DISCUSSION

A. Spectral components

By comparing the effective hydrodynamic radii on different crystal surfaces during various steady-state conditions, two different types of scattering are distinguished (Table I). Radii that are greater than a micrometer are found in almost all crystal systems under a variety of conditions, whereas submicrometer radii are found only on c axis ice and only during the growth process. We observed the submicron or fast spectral component only after carefully controlling the atmospheric conditions in which the samples were prepared. This fast transient has previously been documented in great detail by Böni, Bilgram, and Känzig[5] and Güttinger and co-workers.[10] Bilgram has suggested that this scattering stems from a mesophase layer in between the solid and liquid at the freezing conditions[12] while Keizer, Mazur, and Morita[13] have theorized that the formation and diffusion of a thin layer of dislocations at the growing interface is the source of the scattering.[13]

The slow relaxational component is comprised of objects with radii generally larger than a micrometer and is not unique to the growth process. Data from our experiments supports the mounting evidence that the slow-component scattering results from trapped residual gaseous impurities. According to Cummins, during growth the rejected gaseous impurities eventually leads to supersaturation of gas on the liquid side of the interface followed by heterogeneous nucleation and growth of microbubbles near the crystal surface.[3] Thus the dynamic light scattering experiments are interpreted as measuring the random diffusive motion of these microbubbles.

Our experiments suggest that the segregation of gaseous impurities is not the only source of microbubbles. The slow-decay scattering was always present, to some extent, in our samples even before growth was initiated. We suspect that microbubbles are being deposited by convection near the cell walls during crystal growth. Here they are difficult to detect or remove. The same convective flow may be responsible for the appearance of microbubbles when a molten zone has been created in the crystal. This behavior is probably unique to systems such as the ice-water system where the melt is more dense than the solid.

B. Nonlinearity of Γ versus q^2

The usual process of curve fitting an autocorrelation spectra yields an average linewidth and a variance about this linewidth. Assuming that the scattering is caused by a distribution of different-sized microbubbles, the linewidth is equivalent to an average bubble radius, and the variance measures the polydispersity. If the slow relaxational scattering (large effective radii) is present, it will dominate the spectra since the intensity of the scattered light is proportional to the square of the volume of a microbubble. At forward angles in a polydisperse medium, the geometrical structure factor favors the larger microbubbles and depresses the average linewidth leading to an apparent negative intercept upon extrapolation to $\mathbf{q}=0$.[14] However, the linewidth dependence observed during growth shows an effective *positive* nonzero linewidth, $\Gamma_{q=0}$ (Fig. 1). This can be explained in terms of a phenomenological equation that includes particle diffusion and a local dissipative process with a time constant τ_r. For such a process the Fourier-decomposed

TABLE I. Comparison of hydrodynamic radii for five different systems undergoing relaxational scattering. On growing c-axis ice crystals, the radii were at least 10 times smaller than any other system. In two systems (ice and salol) where the surface was monitored during static, growth, and melt conditions, larger effective radii were found.

Group	System	Radii (μm)	State
Bilgram	Ice (c axis)[a]	0.019–0.079	Growth only
	Salol[b]	0.23–0.38	Growth
Yeh	Ice (a, c axis)	0.33–65.0	Growth, melt, static
	Ice (c axis)	0.059–0.072	Growth only
Cummins[c]	Salol	0.3–4.0	Growth, melt, static[d]
	Cyclohexanol	0.6–3.0	Growth, static
Mesquita[e]	Biphenyl	0.97–3.60	Growth
	Naphthalene	1.65–8.20	Growth

[a]See Ref. 5.
[b]See Ref. 6.
[c]See Ref. 7.
[d]See Ref. 4.
[e]See Ref. 8.

concentration fluctuation, $\delta c(\mathbf{q},t)$, is given by

$$\frac{\partial[\delta c(\mathbf{q},t)]}{\partial t} = -(Dq^2+\tau_r^{-1})\delta c(\mathbf{q},t) , \quad (3)$$

where D is the z-averaged diffusion coefficient. In terms of the microbubble hypothesis $\tau_r^{-1}=\Gamma_{q=0}$ could be interpreted as due to dissipation of bubbles resulting from local "undersaturation" of trapped gases during the growth stage. Because the linewidths are so sensitive to the lateral position on the crystal surface, extrapolation to $\Gamma_{q=0}$ is difficult. This phenomenon deserves closer attention in the future.

Qualitatively, the shapes of the curves of linewidth versus q^2 during various external conditions can also be explained in terms of the microbubble hypothesis. Notice that before growth is initiated the linewidths are small, indicating large average bubble radius. During growth the linewidths increase; this is in agreement with the idea of the nucleation and growth of tiny bubbles that reduce the average bubble size. After growth is arrested, the linewidths start to decrease as there is no longer a mechanism for the production of the smaller bubbles.

C. Liftoff layer

The liftoff phenomena, pictured in Figs. 2(a) and 2(b), can be explained if the attraction among scatterers is greater than the forces attracting them to the receding surface. However, this attraction cannot be stable by itself since it is not strong enough to maintain the layer in the region of above freezing temperature for extended periods of time. For example, compare the median liftoff layer persistence time to the length of time that scattering is recorded from a static crystal surface: The liftoff layer persistence time is around 10 min whereas the scattering from the surface of a crystal allowed to reach static equilibrium has been observed for over 8 h.[9] The time for dissipation of the layer may be determined by the viscous drag on the bubble and the buoyancy force of gravity. After 10 min, an air bubble of 1-μm radius in water will have traveled a distance

$$d = vt = \frac{2r^2 g\,\Delta\rho t}{9\eta} = 1.6 \text{ mm} , \quad (4)$$

where g is the gravitational acceleration, $\Delta\rho$ is the density difference between water and gas, and η is the viscosity of water. Since the waist of our focused laser beam is about 200 μm, these bubbles would disappear from view on the appropriate time scale. In this calculation the possible significant contribution of convection is ignored. Again, these results fit in well with the hypothesis of gaseous microbubbles that would float upwards after being freed from the crystal surface.

D. Hydrodynamic radius and polydispersity

We found a direct relationship between the normalized polydispersity P and the average hydrodynamic radius r_h (Fig. 3). Apparently, crystal growth tends to increase the width of the bubble size distribution as larger bubbles are generated. A direct relationship between polydispersity and hydrodynamic radius seems compatible with the idea of growing microbubbles: Indeed, it is plausible that tiny bubbles nucleate and grow in size, eventually being carried away by their buoyant force or become included into the crystal. As the average bubble size increases, the distribution of bubble size broadens since it includes both the small nucleating bubbles and the larger growing bubbles. On the other hand, when bubbles have just started to nucleate on a clean surface, the distribution of bubbles will be determined by the size at nucleation and tend to be more monodisperse.

V. SUMMARY

We have presented experimental evidence that indicates two types of dynamic light scattering occur at the surface of a growing ice crystal, one fast and one slow. Our data for the fast transient confirms the observations made by Bilgram's group. The slow decaying component exhibits three interesting features: (1) Graphs of Γ versus q^2 suggest that the slow transition does not behave in a strictly self-diffusive manner during growth. (2) A liftoff layer appears during sudden melting of the crystal after a continuous layer of scatterers has been collected on the surface of a growing crystal. This layer appears to break apart as a result of simple gravitational and viscous forces. (3) The direct relationship between polydispersity and the hydrodynamic radius suggests that steady-state crystal growth favors the production of large bubbles is accompanied by a broad distribution of microbubble sizes. The above observations are in qualitative agreement with Cummins's microbubble hypothesis. Our experiments provide evidence supporting the view that the slower decay transient is caused by the nucleation and collection of residual gaseous microbubbles during crystal growth.

It is tempting to draw the conclusion that Bilgram's results are due to a limiting form of bubble formation, where Bilgram's small effective hydrodynamic radii values are consistent with little or no size polydispersity. That explanation, however, fails to clarify the fact that the smallest hydrodynamic radii observed in water adulterated with dissolved gases is more than an order of magnitude larger than observed by Bilgram. It is this missing range of "particle" sizes that suggests there may indeed be two distinct mechanisms for light scattering during the growth of ice crystals: one for bubble formation and one for crystal formation from the pure melt.

ACKNOWLEDGMENTS

We thank C. McDonaugh for the original unpublished observations pertaining to the "liftoff" layer. We are indebted to Professor J. Keizer, Professor P. Mazur, and Professor C. Sorensen for helpful discussions. This work is partially supported by a grant from the National Science Foundation Grant No. CHE-84-05390.

[1]J. H. Bilgram, H. Güttinger, and W. Känzig, Phys. Rev. Lett. **40**, 1394 (1978).

[2]P. N. Pusey, in *Photon Correlation and Light Beating Spectroscopy,* edited by H. Z. Cummins and E. R. Pike (Plenum, New York, 1977), pp. 387–428.

[3]H. Z. Cummins, G. Livescu, H. Chou, and M. R. Srinivasan, Solid State Commun. **60**, 857 (1986).

[4]O. N. Mesquita and H. Z. Cummins, Physico-Chemical Hydrodynamics **5**, 389 (1984).

[5]P. Böni, J. H. Bilgram, and W. Känzig, Phys. Rev. A **28**, 2953 (1983).

[6]U. Dürig, J. H. Bilgram, and W. Känzig, Phys. Rev. A **30**, 946 (1984).

[7]G. Livescu, M. R. Srinivasan, H. Chou, O. Mesquita, and H. Z. Cummins, Phys. Rev. A **36**, 2293 (1987).

[8]O. N. Mesquita, L. O. Ladeira, I. Gontijo, A. G. Oliveria, and G. A. Barbosa, Phys. Rev. B **38**, 1550 (1988).

[9]R. Brown, J. Keizer, U. Steiger, and Y. Yeh, J. Phys. Chem. **87**, 4135 (1983).

[10]H. Güttinger, J. H. Bilgram, and W. Känzig, J. Phys. Chem. Solids **40**, 55 (1979).

[11]*Handbook of Chemistry and Physics* (CRC, Cleveland, OH, 1976).

[12]J. H. Bilgram, Phys. Rep. **153**, 1 (1987).

[13]J. Keizer, P. Mazur, and T. Morita, Phys. Rev. A **32**, 2944 (1985).

[14]Y. Yeh, J. C. Selser, and R. J. Baskin, Biochim. Biphys. Acta **509**, 78 (1978).

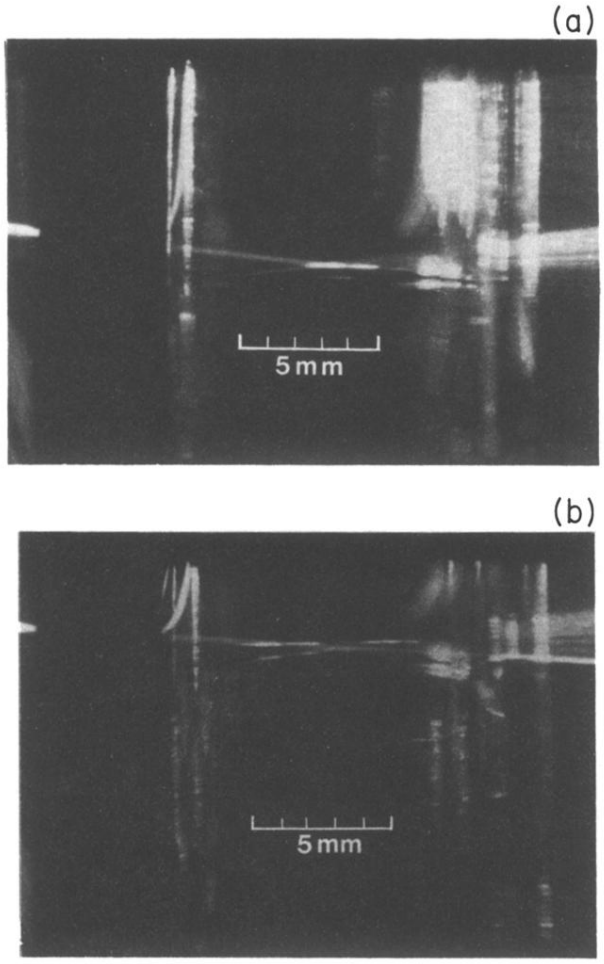

FIG. 2. (a) A crystal at the bottom of the picture is growing into its melt on top (magnification $\approx \times 4$). The crystal surface is the faintly visible concave-down structure appearing horizontally across the center of the photo. The bright white spot in the middle is the 488-nm-wavelength laser beam scattered off the microbubbles in the center of our cell. The straight line entering from the left and reflecting off the surface to the right is the beam as it undergoes Raman scattering from the clear water. (b) Photo of the same cell as in (a) taken 3 min after the ice surface was raised into above-freezing conditions. A liftoff layer of microbubbles appears as the crystal substrate melts underneath a continuous layer of scatterers. A 1-mm gap between the liftoff layer and the surface of the crystal can be seen. There are no scatterers on the surface of the receding crystal; the scattered light observed from the crystal surface represents specular reflection of scattering from the liftoff layer. The temperature gradient is about 10° C/cm.